



HAL
open science

A parallel non-invasive multiscale strategy for a mixed domain decomposition method with frictional contact

Paul Oumaziz, Pierre Gosselet, Pierre-Alain Boucard, Mickaël Abbas

► To cite this version:

Paul Oumaziz, Pierre Gosselet, Pierre-Alain Boucard, Mickaël Abbas. A parallel non-invasive multi-scale strategy for a mixed domain decomposition method with frictional contact. *International Journal for Numerical Methods in Engineering*, 2018, 115 (8), pp.893-912. 10.1002/nme.5830 . hal-01655010

HAL Id: hal-01655010

<https://hal.science/hal-01655010>

Submitted on 4 Dec 2017

HAL is a multi-disciplinary open access archive for the deposit and dissemination of scientific research documents, whether they are published or not. The documents may come from teaching and research institutions in France or abroad, or from public or private research centers.

L'archive ouverte pluridisciplinaire **HAL**, est destinée au dépôt et à la diffusion de documents scientifiques de niveau recherche, publiés ou non, émanant des établissements d'enseignement et de recherche français ou étrangers, des laboratoires publics ou privés.

A parallel non-invasive multiscale strategy for a mixed domain decomposition method with frictional contact

Paul Oumaziz¹, Pierre Gosselet¹, Pierre-Alain Boucard¹, Mickaël Abbas^{2,3}
Submitted to International Journal for Numerical Methods in Engineering

Abstract

A parallel multiscale strategy for a non-invasive mixed domain decomposition method is presented. After briefly exposing our non-invasive implementation of the Latin method, we present how the scalability of the algorithm is obtained by the addition of a global verification of the constitutive law of the interfaces. We propose a new interpretation of the classical macro strategy that impose a global equilibrium of interface's forces. We also propose a new study of a macro strategy that permits to enforce a global continuity of displacement at the interface.

1 Introduction

The industrial simulations of assemblies require to manage complex models with large numbers of degrees of freedom that provokes memory and time consuming limitations. Nonlinearities coming from the complex behaviors, such as plasticity, damage or contact, amplify increasingly the problems of memory or time consumption. Since 80s, domain decomposition methods have been developed to face these issues : Schwarz methods [9], Balancing Domain Decomposition [25], Finite Element Tearing and Interconnecting [8, 7, 6]. They distribute the computation on parallel architecture of hardwares and stretch the memory limitation at the same time they reduce time computation.

The first works on domain decomposition were limited by the scalability of the methods and pathological cases with high heterogeneities. However the recent developments truly improve the robustness of the algorithms. Two-levels algorithms with coarse problems are commonly use [5, 6, 26, 28] and similarities can be done with deflation [29, 14, 33] and multi-grid methods [15, 16, 37]: a comparison can be found in [36]. Adapted augmentation Krylov subspaces obtained through prior quasi-local analysis [35] or multi-preconditioned approaches [11] are also proposed to improve significantly the convergence.

The nonlinearities due to the contact behavior between pieces of an assembly may cause technical difficulties for domain decomposition methods. With the Latin method [17], as subdomains and interfaces are both considered as different entities, it is possible to distinguish the different behaviors, avoiding to verify at the same time, contact laws on interfaces and equilibrium of the linear elastic subdomains. Indeed, the principle of the Latin method is to separate the equations managing contact referring to the interfaces from the equations of equilibrium over subdomains. Therefore two spaces of partial solutions are defined over which a fixed point algorithm is applied to reach the global solution of the problem. Two successive problems are solved at each iteration: a linear stage composed of independent linear elastic problems over subdomains followed by local stage composed of independent nonlinear point-wise problems on interfaces.

The implementation in commercial softwares has becomes one of the issues of these domain decomposition methods. The issue of all these previous methods is their intrusive implementation. Complex development into sources codes are required and even impossible for non opened commercial softwares. Thus, proposing non-intrusive formulation has become a true concern. Works about the global/local

¹LMT/ENS Cachan/CNRS/Université Paris-Saclay
61 avenue du président Wilson 94235 Cachan Cedex FRANCE
{ oumaziz,gosselet,boucard } @lmt.ens-paris-saclay.fr

²EDF R&D
mickael.abbas@edf.fr

³Institut des Sciences de la Mécanique et Applications Industrielles, EDF-CNRS-CEA-ENSTA, Université Paris-Saclay

method have been proposed during the last decade [10, 31, 1, 2]. An extension of this method for a complete domain decomposition for nonlinear problems is described in [4].

For the Latin method, the difficulties come from the mechanical computation under Robin conditions on the boundaries of subdomains which do not incite to develop in the softwares. We propose the scalability of a non-invasive implementation of the Latin method described in [30]. The multiscale strategy of [19, 20] is adapted to this non-invasive approach. A global equilibrium of force distributions is enforced at the linear stage by the introduction of a Lagrange’s multiplier. A macro basis for the displacement of the interface is chosen over which the force is globally equilibrated. Macro information of boundary conditions are directly transmitted through the structure during the iteration improving convergence. The choice of the macro basis is crucial. The optimal one is difficult to choose and it depends on physics of the problem, the geometry and also on boundary conditions [21, 12, 34].

Particularly a new interpretation of the multiscale strategy is proposed. A multiscale modification of the search direction couples all the subdomains together and the method becomes scalable. The algebraic formulation permits to determine precisely the expression of the different projectors and correctly define macro and micro contributions of displacement. A new study of a global continuity strategy is examined. A macro basis for forces is built directly with the first macro basis for displacement. A two-level algorithm is implemented: a first step consists in solving parallel mechanical problems on the subdomains, the second one computes a macro problem that couples subdomains together through an ”homogenized” operator.

This paper is organized as follows: sections 2 and 3 briefly present the substructured problem and the Latin method for a non-invasive mono-scale implementation. The multiscale strategy and its interpretation are presented in section 4. Two approaches are detailed: a global equilibrium and a global continuity strategies. These two strategies are compared on a 3D example in the section 5. The scalability and the influence of the search direction are studied. Finally a severe multiscale frictional 3D case is presented and some performance about the time computation are shown.

2 The substructured reference problem

2.1 substructured discrete problem

We consider an assembly composed of a family of non-overlapping subdomains $(\Omega_E)_{E \in [1, N]}$ of \mathbb{R}^3 . We assume small perturbations and quasi-static isotherm evolution. The material is supposed to be isotropic linear elastic; Hooke’s tensor \mathbb{K} is characterized by Young’s modulus and Poisson’s ratio. We use classical Lagrange conforming finite element. We denote by \mathbf{K}_E the stiffness matrix related to the subdomain Ω_E , by \mathbf{u}_E the vector of nodal displacement over the subdomain, and by \mathbf{f}_{dE} the generalized forces associated to given loads. Degrees of freedom submitted to Dirichlet boundary conditions are supposed to having been eliminated.

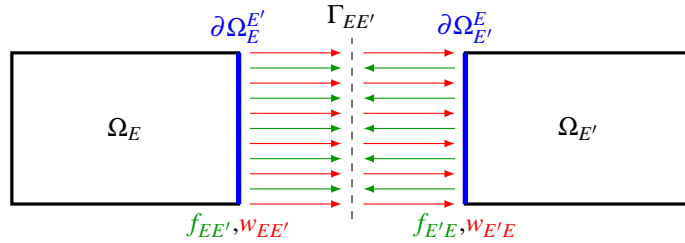


Figure 1: Force and displacement fields defined on the edges of the subdomains

Subdomain Ω_E interacts with any neighboring subdomain $\Omega_{E'}$ through the interface $\Gamma_{EE'}$. For each interface we introduce finite element displacement and force distributions defined on the edges of the related subdomains: $(\mathbf{w}_{EE'}, \mathbf{w}_{E'E})$ and $(\mathbf{f}_{EE'}, \mathbf{f}_{E'E})$. These fields are connected to the subdomains’ by trace relations materialized by the operator $\mathbf{N}_{EE'}$. Let \mathcal{E} be the set of all subdomains and \mathcal{G} the set of all interfaces.

We use (pseudo)-time in order to properly describe complex load sequences and to be able to manage the history-dependence of the solution. We use dot notations $(\dot{\mathbf{w}}_{EE'}, \dot{\mathbf{u}}_E)$ for the interface and

subdomain velocity fields. In practice a simple backward Euler scheme is used for the time integration.

To easily handle the many interfaces of one subdomain, we define concatenated operators:

$$\mathbf{w}_E = \begin{pmatrix} \vdots \\ \mathbf{w}_{EE'} \\ \vdots \end{pmatrix}, \quad \mathbf{f}_E = \begin{pmatrix} \vdots \\ \mathbf{f}_{EE'} \\ \vdots \end{pmatrix}, \quad \mathbf{N}_E = \begin{pmatrix} \ddots & & \\ & \mathbf{N}_{EE'} & \\ & & \ddots \end{pmatrix}, \quad E' \text{ spans all neighbors} \quad (1)$$

The mechanical problems to solve on the subdomains is:

$$\text{subdomains: } \forall \Omega_E \in \mathcal{E}, \forall t, \quad \begin{cases} \mathbf{K}_E \mathbf{u}_E^t = \mathbf{f}_{dE}^t + \mathbf{N}_E^T \mathbf{f}_E^t \\ \mathbf{w}_E^t = \mathbf{N}_E \mathbf{u}_E^t \end{cases} \quad (2)$$

The mechanical behavior of the interface $\Gamma_{EE'}$ can be given by a relation of the form:

$$\text{Interfaces: } \forall \Gamma_{EE'} \in \mathcal{G}, \quad \begin{cases} \mathbf{f}_{EE'}^t + \mathbf{f}_{E'E}^t = 0, \forall t \\ \mathbf{f}_{EE'}^t = \mathbf{b}_{EE'} \left(\dot{\mathbf{w}}_{E'E}^{t'} - \dot{\mathbf{w}}_{EE'}^{t'}, t' \leq t; \mathbf{w}_{E'E}^0 - \mathbf{w}_{EE'}^0 \right), \forall t \\ \text{Initial conditions} \end{cases} \quad (3)$$

where the first relation is the balance of forces and the second relation represents the constitutive law of the mechanical behavior. Intuitively, perfect and contact interfaces can be considered as limit cases of mechanical behaviors (3) (think of a perfect interface as an infinitely stiff interface). In the following we use the term ‘‘interface behavior’’ and the notation $\mathbf{b}_{EE'}$ for any kind of interface, except when being more specific is required.

2.2 Assembly operators and perfect interfaces

Block notations are used to simplify the writing of all the relations. As said earlier \mathbf{x}_E represents the gathering of all the $(\mathbf{x}_{EE'})_{E'}$. \mathbf{x} will represent the gathering of all the \mathbf{x}_E defined on each subdomain Ω_E , same procedure applies to operators:

$$\mathbf{x} = \begin{pmatrix} \vdots \\ \mathbf{x}_E \\ \vdots \end{pmatrix}, \quad \mathbf{K} = \begin{pmatrix} \ddots & & 0 \\ & \mathbf{K}_E & \\ 0 & & \ddots \end{pmatrix}, \quad \text{where } E \text{ spans all subdomains} \quad (4)$$

We introduce operators which permit to make neighboring subdomains communicate: the operator \mathbf{A} makes sum of interface vectors whereas the operator \mathbf{B} makes differences:

$$\begin{aligned} (\mathbf{A}\mathbf{f})_{|\Gamma_{EE'}} &= \mathbf{f}_{EE'} + \mathbf{f}_{E'E} \\ (\mathbf{B}\mathbf{w})_{|\Gamma_{EE'}} &= \mathbf{w}_{E'E} - \mathbf{w}_{EE'} \end{aligned} \quad (5)$$

These operators are orthogonal in the sense that $\ker(\mathbf{A}) = \text{range}(\mathbf{B}^T)$.

2.3 Discrete problem

Under these notations, the discrete problem equivalent to the substructured problem is:

$$\forall t, \quad \begin{cases} \mathbf{K}\mathbf{u}^t = \mathbf{f}_d^t + \mathbf{N}^T \mathbf{f}^t & \text{Equilibrium of the subdomains} \\ \mathbf{w}^t = \mathbf{N}\mathbf{u}^t & \text{Trace of the subdomain displacement} \\ \mathbf{f}^t = \mathbf{B}^T \mathbf{b}(\mathbf{B}\dot{\mathbf{w}}^{t'}, t' \leq t, \mathbf{B}\mathbf{w}^0) & \text{Interfaces' behavior} \end{cases} \quad (6)$$

This notation for the interface’s behavior makes it clear that the equilibrium is ensured: $\mathbf{A}\mathbf{f} = \mathbf{A}\mathbf{B}^T \mathbf{b}(\mathbf{B}\mathbf{w}) = 0$. Note that in the case of perfect interfaces, the equations become:

$$\forall t, \quad \begin{cases} \mathbf{A}\mathbf{f}^t = 0 \\ \mathbf{B}\mathbf{w}^t = 0 \end{cases} \quad (7)$$

The contact formulation with Coulomb friction is fully detailed in [30].

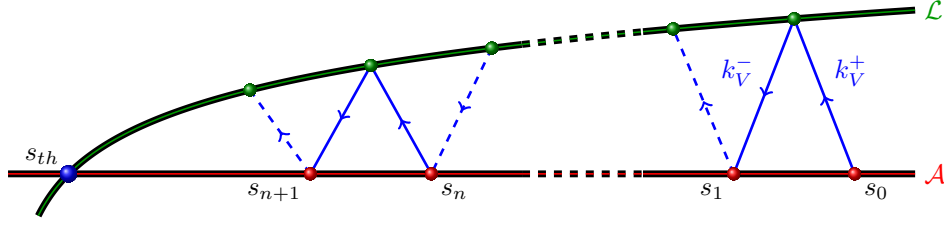


Figure 2: Latin method

3 The non-invasive Latin method

3.1 Principle of the Latin method

In order to solve the problem (6), we use the Latin method [17] which is a variant of the method of alternate search directions. We define two sets of interface fields:

$$\mathcal{A} : (\mathbf{f}^t, \dot{\mathbf{w}}^t)_t \text{ solutions to } \forall t \begin{cases} \mathbf{K}\mathbf{u}^t = \mathbf{f}_d^t + \mathbf{N}^T \mathbf{f}^t \\ \dot{\mathbf{w}}^t = \mathbf{N}\dot{\mathbf{u}}^t \\ \dot{\mathbf{u}}^t = (\mathbf{u}^t - \mathbf{u}^{t-\Delta t})/\Delta t, + \text{initial condition} \end{cases} \quad (8)$$

$$\mathcal{L} : (\hat{\mathbf{f}}^t, \hat{\mathbf{w}}^t)_t \text{ solutions to } \forall t \hat{\mathbf{f}}^t = \mathbf{B}^T \mathbf{b}(\mathbf{B}\hat{\mathbf{w}}^t, t' \leq t, \mathbf{B}\hat{\mathbf{w}}^t) \quad (9)$$

The set \mathcal{A} is made out of solutions to linear equations set on subdomains, it is thus an affine space often called space of admissible fields. The set \mathcal{L} is in general a manifold (in the case of perfect interfaces, it is a vector space), one important feature is that the equations which define it are pointwise independent in time and space (they are often called “local” equations).

The solution is reached by iterations where partial solutions are alternatively searched for in each set \mathcal{A} and \mathcal{L} .

Starting from a partial solution $s_n = (\mathbf{f}_n, \dot{\mathbf{w}}_n) \in \mathcal{A}$, the so-called *local stage* consists in searching for a partial solution $\hat{s}_n = (\hat{\mathbf{f}}_n, \hat{\mathbf{w}}_n) \in \mathcal{L}$. This is made possible by enforcing a search direction of the form:

$$\mathbf{f}_n - \hat{\mathbf{f}}_n - \mathbf{k}_V^+ (\dot{\mathbf{w}}_n - \hat{\mathbf{w}}_n) = 0 \quad (10)$$

where \mathbf{k}_V^+ is an operator which can be chosen by the user. In order to benefit the local character of the equations which define \mathcal{L} , \mathbf{k}_V^+ is often chosen to be diagonal.

Starting from a partial solution $\hat{s}_n = (\hat{\mathbf{f}}_n, \hat{\mathbf{w}}_n) \in \mathcal{L}$, the so-called *linear stage* consists in searching for a partial solution $s_{n+1} = (\mathbf{f}_{n+1}, \dot{\mathbf{w}}_{n+1}) \in \mathcal{A}$. This is made possible by enforcing a search direction of the form:

$$\mathbf{f}_{n+1} - \hat{\mathbf{f}}_n + \mathbf{k}_V^- (\dot{\mathbf{w}}_{n+1} - \hat{\mathbf{w}}_n) = 0 \quad (11)$$

where \mathbf{k}_V^- is an operator which can be chosen by the user.

The iterations are graphically represented on Figure 2. A relaxation is often applied at the end of linear stages:

$$s_{n+1} \leftarrow s_n + \alpha(s_{n+1} - s_n) \quad (12)$$

with $0 < \alpha \leq 1$.

Proposition 1 *The convergence of $(s_{n+1} + s_n)/2$ is proved in [17] when $\mathbf{k}_V^- = \mathbf{k}_V^+$ are symmetric definite positive operators and $\alpha < 1$ for maximal monotone behaviors \mathbf{b} .*

3.2 The non-invasive implementation

During the linear stage, independent solves on the subdomains are performed. Equations (8) and (11) lead to the following equations which are independent per subdomain, and where $(\hat{\mathbf{f}}^{t+\Delta t}, \hat{\mathbf{w}}^{t+\Delta t})$ are known from previous local stage:

$$\left(\mathbf{K} + \mathbf{N}^T \frac{\mathbf{k}_V^-}{\Delta t} \mathbf{N} \right) \mathbf{u}^{t+\Delta t} = \mathbf{f}_d^{t+\Delta t} + \mathbf{N}^T \left(\hat{\mathbf{f}}^{t+\Delta t} + \mathbf{k}_V^- \hat{\mathbf{w}}^{t+\Delta t} + \frac{\mathbf{k}_V^-}{\Delta t} \mathbf{w}^t \right) \quad (13)$$

$$\text{Then compute } \begin{cases} \dot{\mathbf{w}}^{t+\Delta t} &= \mathbf{N} \dot{\mathbf{u}}^{t+\Delta t} = \mathbf{N}(\mathbf{u}^{t+\Delta t} - \mathbf{u}^t) / \Delta t \\ \mathbf{f}^{t+\Delta t} &= \hat{\mathbf{f}}^{t+\Delta t} + \mathbf{k}_V^- \left(\hat{\mathbf{w}}^{t+\Delta t} - \dot{\mathbf{w}}^t \right) \end{cases} \quad (14)$$

Remark 1 Equation (13) can be interpreted as the discretization of the subdomains equilibrium under a generalized Robin boundary condition. The term $(\mathbf{N}^T \mathbf{k}_V^- \mathbf{N})$ in (13) corresponds to the interface impedance, it is a non-standard term in industrial finite elements software for mechanical problems (there often exist implementations for thermal problems, since it corresponds to convection conditions).

A new implementation of the generalized Robin conditions is needed to tackle the constraints of industrial finite elements software. Several proposals are given in [30]. We choose to consider $\mathbf{k}^- = \mathbf{k}_V^- / \Delta t$ as a generalized Robin condition which can be realized by adding matter on the boundary of the subdomains. This strategy leads to a “non-local” search direction in the sense that the nodes of an interface are coupled together through the layer of elements (\mathbf{k}^- is not diagonal).

The matter added at interface $\Gamma_{EE'}$ is written $\theta_{EE'}$, the Hooke tensor associated to its behavior is $\mathbb{K}_{\theta_{EE'}}$. The addition is called a “sole”. A zero Dirichlet condition is imposed on the part $\partial_u \mathbb{K}_{\theta_{EE'}}$ of the boundary of the sole which is not in contact with the interface. $\mathbf{K}_{\theta_{EE'}}$ is the stiffness matrix of the sole (with zero Dirichlet boundary conditions taken into account). $\mathbf{k}_{EE'}^-$ is the Schur complement of $\mathbf{K}_{\theta_{EE'}}$ which condenses the stiffness on the interface degrees of freedom.

Remark 2 (Practical considerations)

- In order not to enlarge computations, we choose to add only one layer of elements. With such a choice and in the case of linear elements, as the zero Dirichlet boundary conditions are eliminated, the Schur complement is strictly equal to the stiffness operator $\mathbf{K}_{\theta_{EE'}}^- = \mathbf{k}_{EE'}^-$.
- The search direction is parametrized by the behavior of the sole. We chose to use the same Poisson’s ratio as the subdomain and to adapt the Young modulus. Classically the search direction is chosen such as $\mathbf{k} = Y/L$ [17] with Y the Young modulus of the structure and L a characteristic length of the structure. In our case, the idea is kept and the Young modulus of the sole is chosen such as

$$\frac{Y_S}{L_S} = \frac{Y}{L} \quad (15)$$

with Y_S the Young modulus of the sole and L_S a characteristic width of the sole.

With this non-invasive search direction, solving the problem of the linear stage $(\mathbf{K} + \mathbf{N}^T \mathbf{k}^- \mathbf{N})$ amounts to solve a mechanical problem on subdomain extended with the sole, loaded by an inner interface traction field (Figure 3). This stiffness assembly is a classical operation in commercial softwares.

3.3 Control of convergence

An error indicator η can be defined to control the convergence of the method. This indicator represents the distance between a local solution in \mathcal{L} and a linear solution in \mathcal{A} :

$$\eta = \frac{\sum_t \left(\dot{\mathbf{w}}^t - \hat{\mathbf{w}}^t \right)^T \mathbf{k}_V^- \left(\dot{\mathbf{w}}^t - \hat{\mathbf{w}}^t \right) + \sum_t \left(\mathbf{f}^t - \hat{\mathbf{f}}^t \right)^T \mathbf{k}_V^{-1} \left(\mathbf{f}^t - \hat{\mathbf{f}}^t \right)}{\sum_t \left(\dot{\mathbf{w}}^t \mathbf{k}_V^- \dot{\mathbf{w}}^t + \mathbf{f}^t \mathbf{k}_V^{-1} \mathbf{f}^t + \hat{\mathbf{w}}^t \mathbf{k}_V^- \hat{\mathbf{w}}^t + \hat{\mathbf{f}}^t \mathbf{k}_V^{-1} \hat{\mathbf{f}}^t \right)} \quad (16)$$

Remark 3 (Properties of the indicator)

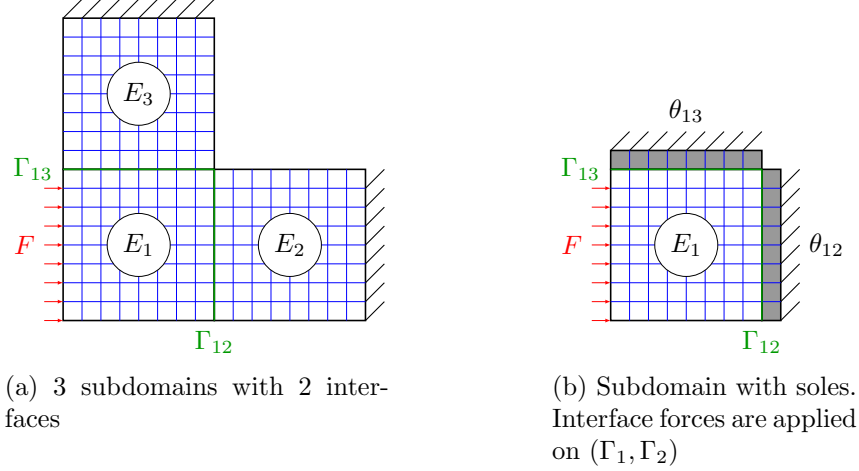


Figure 3: Example of a problem to solve at linear stage

- The indicator is post-processed from the linear stage.
- The indicator depends on the search direction.
- Other indicators based on true errors $\mathbf{A}\mathbf{f}$ and $\mathbf{B}\hat{\mathbf{w}}$, which are computed at the beginning of the local step can also be used.

4 The multiscale strategy in the Latin method

The multiscale strategy is presented in this section. During the linear stage, displacement and force distributions do not verify the constitutive law of the interface. With perfect interface, before convergence we have : $\mathbf{B}\hat{\mathbf{w}} \neq 0$ and $\mathbf{A}\mathbf{f} \neq 0$. Thus the idea is to modify the linear stage in order to enforce a “global” verification of the constitutive law.

Firstly we explain the classical definition of a macro space for displacement that results in a global weak equilibrium of the force distributions over the whole structure. A new interpretation is detailed to show that this two-level strategy can be seen as a particular choice of the search direction. The algebraic notations permits to bring out the micro / macro space for distributions of interface.

Finally an explanation of the computation of the “macro” operator and the resolution of the multiscale approach is presented.

4.1 The multiscale strategy with global equilibrium

4.1.1 Definition of a macro space for displacement.

A macro basis of interface displacement is chosen over which force will be globally equilibrated. The macro basis of the interface $\Gamma_{EE'}$ is denoted $\mathbb{W}_{EE'}$ and the associated macro space is $\mathcal{W}_{EE'}^M = \text{span}(\mathbb{W}_{EE'})$. This macro space has to be orthogonal to the force distributions which propagate deeply in the structure. In agreement with Saint Venant’s principle, the macro basis consists of rigid body motions, it is completed with simple deformation modes such as extension and shearing modes (Figure 4).

4.1.2 Definition of the linear stage

The global equilibrium is enforced by the addition of a constraint to the linear problem. With the block notations for \mathbb{W} this relation is:

$$\mathbb{W}^T \mathbf{A}\mathbf{f} = 0 \tag{17}$$

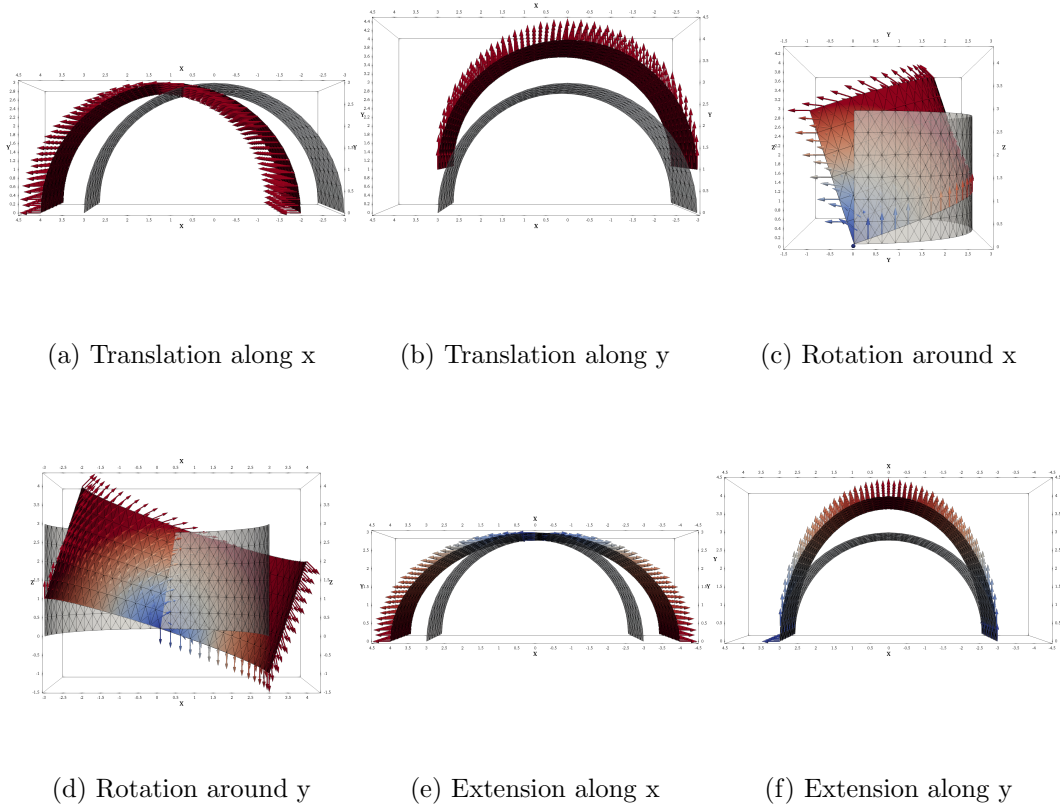


Figure 4: Examples of macro displacement modes

It imposes to reconsider the search direction which is now defined globally over all the interfaces and no more separately on each interface:

$$\min_{\mathbb{W}^T \mathbf{A} \mathbf{f} = 0} \left[\frac{1}{2} (\mathbf{f} - \widehat{\mathbf{f}})^T \mathbf{k}_V^{-1} (\mathbf{f} - \widehat{\mathbf{f}}) + (\mathbf{f} - \widehat{\mathbf{f}})^T (\dot{\mathbf{w}} - \widehat{\dot{\mathbf{w}}}) \right] \quad (18)$$

The constraint is taken into account by the definition of a lagrangian whose stationarity leads to:

$$(\mathbf{f} - \widehat{\mathbf{f}}) + \mathbf{k}_V^{-1} (\dot{\mathbf{w}} - \widehat{\dot{\mathbf{w}}}) + \mathbf{k}_V^{-1} \mathbf{A}^T \mathbb{W} \alpha = 0 \quad (19)$$

where α is the Lagrange multiplier.

Remark 4 Classically in [18, 19], the multiplier corresponds to $\mathbb{W}^T \mathbf{A} \alpha$ and it is written \tilde{W} .

With the quasi-static assumption the problem of the linear stage can be written as:

Find $(\mathbf{w}^{t+\Delta t}, \dot{\mathbf{w}}^{t+\Delta t}, \mathbf{f}^{t+\Delta t})$ solution to :

$$\begin{cases} \mathbf{K} \mathbf{u}^{t+\Delta t} = \mathbf{f}_d + \mathbf{N}^T \mathbf{f}^{t+\Delta t} \\ \dot{\mathbf{w}}^{t+\Delta t} = \mathbf{N} \dot{\mathbf{u}}^{t+\Delta t} = \mathbf{N} (\mathbf{u}^{t+\Delta t} - \mathbf{u}^t) / \Delta t \\ \mathbb{W}^T \mathbf{A} \mathbf{f}^{t+\Delta t} = 0 \\ (\mathbf{f}^{t+\Delta t} - \widehat{\mathbf{f}}^{t+\Delta t}) + \mathbf{k}_V^{-1} (\dot{\mathbf{w}}^{t+\Delta t} - \widehat{\dot{\mathbf{w}}}^{t+\Delta t}) + \mathbf{k}_V^{-1} \mathbf{A}^T \mathbb{W} \alpha^{t+\Delta t} = 0 \end{cases} \quad (20)$$

4.1.3 New interpretation of the multiscale strategy

We first apply the operator $\mathbb{W}^T \mathbf{A}$ on the relation of search direction to remove the unknown $\mathbf{f}^{t+\Delta t}$:

$$\underbrace{\mathbb{W}^T \mathbf{A} \mathbf{f}^{t+\Delta t}}_{=0 \text{ (macro equilibrium)}} - \mathbb{W}^T \underbrace{\mathbf{A} \widehat{\mathbf{f}}^{t+\Delta t}}_{=0 \text{ (local equilibrium)}} + \mathbb{W}^T \mathbf{A} \mathbf{k}_V^{-1} (\dot{\mathbf{w}}^{t+\Delta t} - \widehat{\dot{\mathbf{w}}}^{t+\Delta t}) + \mathbb{W}^T \mathbf{A} \mathbf{k}_V^{-1} \mathbf{A}^T \mathbb{W} \alpha^{t+\Delta t} = 0 \quad (21)$$

Thus the multiplier is expressed in function of the unknown velocity $\dot{\mathbf{w}}^{t+\Delta t}$:

$$\alpha^{t+\Delta t} = (\mathbb{W}^T \mathbf{A} \mathbf{k}_V^- \mathbf{A}^T \mathbb{W})^{-1} \left[\mathbb{W}^T \mathbf{A} \mathbf{k}_V^- \left(\hat{\mathbf{w}}^{t+\Delta t} - \dot{\mathbf{w}}^{t+\Delta t} \right) \right] \quad (22)$$

Afterwards the multiplier is injected in the search direction to express the unknown $\mathbf{f}^{t+\Delta t}$ in function of the velocity unknown $\dot{\mathbf{w}}^{t+\Delta t}$:

$$\mathbf{f}^{t+\Delta t} = \mathbf{k}_V^- \left[\mathbb{I} - \mathbf{A}^T \mathbb{W} (\mathbb{W}^T \mathbf{A} \mathbf{k}_V^- \mathbf{A}^T \mathbb{W})^{-1} \mathbb{W}^T \mathbf{A} \mathbf{k}_V^- \right] \left(\hat{\mathbf{w}}^{t+\Delta t} - \dot{\mathbf{w}}^{t+\Delta t} \right) + \hat{\mathbf{f}}^{t+\Delta t} \quad (23)$$

With this new expression of the search direction and the Euler scheme, we obtain the following problem written in displacement to compute $\mathbf{u}^{t+\Delta t}$:

$$\boxed{\begin{aligned} \left[\mathbf{K} + \mathbf{N}^T \frac{\mathbf{k}_V^-}{\Delta t} (\mathbb{I} - \mathbf{P}_M) \mathbf{N} \right] \mathbf{u}^{t+\Delta t} &= \mathbf{f}_d + \mathbf{N}^T \hat{\mathbf{f}}^{t+\Delta t} + \mathbf{N}^T \mathbf{k}_V^- (\mathbb{I} - \mathbf{P}_M) \left[\hat{\mathbf{w}}^{t+\Delta t} + \frac{\mathbf{w}^t}{\Delta t} \right] \\ \text{with } \mathbf{P}_M &= \mathbf{A}^T \mathbb{W} (\mathbb{W}^T \mathbf{A} \mathbf{k}_V^- \mathbf{A}^T \mathbb{W})^{-1} \mathbb{W}^T \mathbf{A} \mathbf{k}_V^- \end{aligned}} \quad (24)$$

Remark 5 (Properties of the projection)

- \mathbf{P}_M is the macro projector which is applied to the displacement. Its definition only involves the search direction and the macro basis; it is not connected to the properties of the real structure.
- The multiscale approach has thus two effects: it propagates the right-hand side and it softens the Robin condition in the left-hand side by a low-rank term.
- $\mathbf{P}_m = \mathbb{I} - \mathbf{P}_M$ is a micro projector filtering the macro part of the displacement. The algebraic properties of this micro projector imply that the micro part of the displacement and the macro part of the force are orthogonal.

$$\begin{aligned} \ker(\mathbf{P}_m) &= \text{range}(\mathbf{A}^T \mathbb{W}) \quad \text{filters out the macro part of displacement} \\ \text{Im}(\mathbf{P}_m) &= \ker(\mathbb{W}^T \mathbf{A} \mathbf{k}^-) \end{aligned} \quad (25)$$

- It makes sense to define a macro subspace of forces: $\mathcal{F}^M = \text{span}(\mathbf{k}^- \mathbf{A}^T \mathbb{W}) = \text{range}(\mathbf{P}_m)^\perp$. This macro force space is not balanced between subdomains except when search directions \mathbf{k}^- are identical between neighboring subdomains.

4.1.4 Illustration of the multiscale effect on the linear problem

By considering the structure described at Figure 3, the macro constraint modifies the stiffness operator (which is initially block-diagonal) by out-diagonal terms as illustrated on Figure 5. The factorization of the operator permits to propagate the information of the boundary condition included in the right-hand side to all the subdomains.

4.2 Computation of the multiscale stiffness operator and resolution

In order to use a parallel resolution over the subdomains, it is impossible to invert directly $\left[\mathbf{K} + \mathbf{N}^T \frac{\mathbf{k}_V^-}{\Delta t} (\mathbb{I} - \mathbf{P}_M) \mathbf{N} \right]$. Indeed the macro projector couples the subdomains together and therefore this operator becomes global over all the subdomains. Instead, the inverse of the operator is expressed with the identity of Woodbury [38]:

$$(M + UCV)^{-1} = M^{-1} - M^{-1}U(C^{-1} + VM^{-1}U)^{-1}VM^{-1} \quad (26)$$

In our case we have:

$$\begin{cases} M = \mathbf{K} + \mathbf{N}^T \frac{\mathbf{k}_V^-}{\Delta t} \mathbf{N} \\ C = - \left(\mathbb{W}^T \mathbf{A} \frac{\mathbf{k}_V^-}{\Delta t} \mathbf{A}^T \mathbb{W} \right)^{-1} \\ U = V^T = \mathbf{N}^T \mathbf{k}_V^- \mathbf{A}^T \mathbb{W} \end{cases} \quad (27)$$

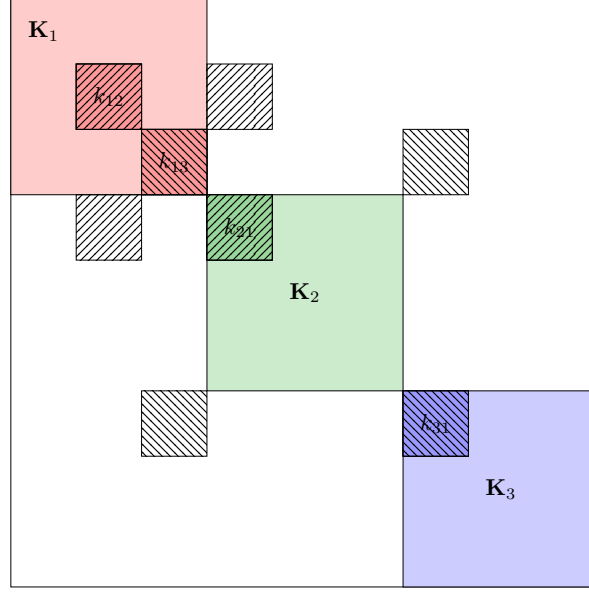


Figure 5: Block stiffness operator with out-diagonal terms due to the macro projector

Noting $\tilde{\mathbf{k}} = \mathbf{N}^T \frac{\mathbf{k}_V^-}{\Delta t} \mathbf{N}$ the inverse of the global stiffness operator becomes:

$$\begin{aligned} \mathbf{K}_{tot}^{-1} &= \left(\mathbf{K} + \tilde{\mathbf{k}} \right)^{-1} - \left(\mathbf{K} + \tilde{\mathbf{k}} \right)^{-1} \mathbf{N}^T \mathbf{k}_V^- \mathbf{A}^T \mathbb{W} \dots \\ &\dots \left(\mathbb{W}^T \mathbf{A} \left[\mathbf{k}_V^- \mathbf{N} \left(\mathbf{K} + \tilde{\mathbf{k}} \right)^{-1} \mathbf{N}^T - \mathbb{I} \right] \mathbf{k}_V^- \mathbf{A}^T \mathbb{W} \right)^{-1} \dots \\ &\dots \mathbb{W} \mathbf{A} \mathbf{k}_V^- \mathbf{N} \left(\mathbf{K} + \tilde{\mathbf{k}} \right)^{-1} \end{aligned} \quad (28)$$

Therefore the expression of the displacement becomes:

$$\begin{aligned} \mathbf{u}^{t+1} &= \left[\left(\mathbf{K} + \tilde{\mathbf{k}} \right)^{-1} - \left(\mathbf{K} + \tilde{\mathbf{k}} \right)^{-1} [\dots] \left(\mathbf{K} + \tilde{\mathbf{k}} \right)^{-1} \right] \dots \\ &\dots \left(\mathbf{f}_d + \mathbf{N}^T \left(\hat{\mathbf{f}}^{t+\Delta t} + \mathbf{k}_V^- (\mathbb{I} - \mathbf{P}_M) \left[\hat{\mathbf{w}}^{t+\Delta t} + \frac{\mathbf{w}^t}{\Delta t} \right] \right) \right) \end{aligned} \quad (29)$$

According to the expression of the inverse of the global stiffness operator, a two-steps strategy is adopted. The first step is a parallel computation over each subdomains. It consists in solving:

$$\left(\mathbf{K} + \tilde{\mathbf{k}} \right) \mathbf{u}_1^{t+1} = \mathbf{f}_d + \mathbf{N}^T \left(\hat{\mathbf{f}} + \mathbf{k}_V^- \left[\hat{\mathbf{w}}^{t+\Delta t} + \frac{\mathbf{w}^t}{\Delta t} \right] \right) \quad (30)$$

In the second step, a macro correction is computed:

$$\begin{aligned} \mathbf{u}_2^{t+1} &= -\mathbb{V} \mathbf{K}_2^{-1} (\mathbb{W}^T \mathbf{A} \mathbf{F}_2) \\ \text{with } \mathbb{V} &= \left(\mathbf{K} + \tilde{\mathbf{k}} \right)^{-1} \mathbf{N}^T \mathbf{k}_V^- \mathbf{A}^T \mathbb{W} \\ \mathbf{K}_2 &= \mathbb{V}^T \mathbf{N}^T \mathbf{k}_V^- \mathbf{A}^T \mathbb{W} - \mathbb{W}^T \mathbf{A} \mathbf{k}_V^- \mathbf{A}^T \mathbb{W} \\ \mathbf{F}_2 &= \mathbf{k}_V^- \left(\hat{\mathbf{w}}^{t+\Delta t} + \frac{\mathbf{w}^t}{\Delta t} - \frac{\mathbf{N} \mathbf{u}_1^{t+1}}{\Delta t} \right) \end{aligned} \quad (31)$$

Then the displacement is:

$$\mathbf{u}^{t+1} = \mathbf{u}_1^{t+1} + \mathbf{u}_2^{t+1} \quad (32)$$

Remark 6

- \mathbf{K}_2 is computed at the beginning of the algorithm and called "macro" operator in [19, 20]. It consists in determining successively the behavior of the subdomains under macro load from the macro basis of displacement. That is why it is often referred as the homogenized behavior of the subdomains. During the computation of \mathbf{K}_2 , the basis \mathbb{V} is stored on the subdomains.
- The computation of $(\mathbb{W}^T \mathbf{A} \mathbf{F}_2)$ requires a global reduction at each iteration.
- One can remark that the Lagrange's multiplier can be expressed as :

$$\alpha^{t+\Delta t} = \mathbf{K}_2^{-1} \mathbb{W}^T \mathbf{A} \mathbf{F}_2 \quad (33)$$

which is computed during the second step. Therefore, the computation of $\mathbf{f}^{t+\Delta t}$ does not require any supplementary communication.

The method is summed up in the algorithm 1.

Algorithm 1: Multiscale Latin method with global weak equilibrium of force

Input: Initialisation

Factorization of the "macro" operator:

$$\mathbf{K}_2 = \mathbb{W}^T \mathbf{A} \left(\mathbf{k}_V^- \mathbf{N} \left(\mathbf{K} + \tilde{\mathbf{k}} \right)^{-1} \mathbf{N}^T - \mathbb{I} \right) \mathbf{k}_V^- \mathbf{A}^T \mathbb{W}$$

Saving of the intermediate quantity:

$$\mathbb{V} = \left(\mathbf{K} + \tilde{\mathbf{k}} \right)^{-1} \mathbf{N}^T \mathbf{k}_V^- \mathbf{A}^T \mathbb{W}$$

while Error criterion < objective **do**

Local stage:

foreach time step **do**

foreach interface **do**

 | Interface computation detailed in [30]

end

end

Linear stage:

foreach time step **do**

foreach subdomain **do**

 1. Parallel computation on subdomains

$$\mathbf{u}_1^{t+1} = \left(\mathbf{K} + \tilde{\mathbf{k}} \right)^{-1} \left[\mathbf{F}_d + \mathbf{N}^T \left(\hat{\mathbf{f}} + \mathbf{k}_V^- \left[\hat{\mathbf{w}}^{t+\Delta t} + \frac{\mathbf{w}^t}{\Delta t} \right] \right) \right]$$

 2. Communication between subdomains and second parallel computation

$$\text{Communication to compute } \psi = \mathbb{W}^T \mathbf{A} \mathbf{k}_V^- \left(\hat{\mathbf{w}}^{t+\Delta t} + \frac{\mathbf{w}^t}{\Delta t} - \frac{\mathbf{N} \mathbf{u}_1^{t+1}}{\Delta t} \right)$$

 Save of the multiplier: $\alpha^{t+\Delta t} = \mathbf{K}_2^{-1} \psi$

 Parallel computation: $\mathbf{u}_2^{t+1} = -\mathbb{V} \alpha^{t+\Delta t}$

 Finally: $\mathbf{u}^{t+1} = \mathbf{u}_1^{t+1} + \mathbf{u}_2^{t+1}$

 3. Computation of interface's distributions

 Time scheme to compute velocity: $\dot{\mathbf{w}}^{t+\Delta t} = (\mathbf{w}^{t+\Delta t} - \mathbf{w}^t) / \Delta t$

 Search direction to compute force: $\mathbf{f}^{t+\Delta t} = \hat{\mathbf{f}}^{t+\Delta t} - \mathbf{k}_V^- \left(\dot{\mathbf{w}}^{t+\Delta t} - \hat{\mathbf{w}}^{t+\Delta t} \right) - \mathbf{k}_V^- \mathbf{A}^T \mathbb{W} \alpha^{t+\Delta t}$

 4. Relaxation step

$s_{n+1} \leftarrow s_n + \alpha (s_{n+1} - s_n)$;

end

end

end

4.3 A macro strategy for the weak continuity of displacement

In the case of perfect interfaces, it makes sense to impose a weak continuity of the displacement. This weak continuity is defined by the orthogonality to a macro basis in force:

$$\mathbb{F}^T \mathbf{B} \mathbf{w} = 0 \quad (34)$$

Note that such a strategy was evoked in [19] and a study of optimal search direction was proposed. However the extensibility was not illustrated. In this paper we proposed to complete this approach by formulate it under algebraic notations. This reveals some properties of the different operators and facilitate the analyze of the extensibility results.

4.3.1 Definition of a macro space for force

The choice of the force macro basis is far from trivial, in particular if we wish to adapt to irregular interfaces. The more advanced strategies can be found in FETIDP-BDDC literature [27, 13, 32].

For now, we adopt a simple strategy by simply processing the displacement macro basis:

$$\mathbb{F} := \left(\mathbf{A} \frac{\mathbf{k}_V^-}{\Delta t} \mathbf{A}^T \right) \mathbb{W} \quad (35)$$

4.3.2 Definition of the linear stage

In order to comply with the macro constraint (which also applies to the velocities), the search direction is seen a minimization:

$$\begin{aligned} \min_{\mathbb{F}^T \mathbf{B} \dot{\mathbf{w}}^{t+\Delta t} = 0} & \left[\left(\dot{\mathbf{w}}^{t+\Delta t} - \widehat{\mathbf{w}}^{t+\Delta t} \right)^T \left(\mathbf{f}^{t+\Delta t} - \widehat{\mathbf{f}}^{t+\Delta t} \right) \dots \right. \\ & \left. + \dots \frac{1}{2} \left(\dot{\mathbf{w}}^{t+\Delta t} - \widehat{\mathbf{w}}^{t+\Delta t} \right)^T \mathbf{k}_V^- \left(\dot{\mathbf{w}}^{t+\Delta t} - \widehat{\mathbf{w}}^{t+\Delta t} \right)^T \right] \end{aligned} \quad (36)$$

which leads to the following search direction:

$$\mathbf{f}^{t+\Delta t} - \widehat{\mathbf{f}}^{t+\Delta t} + \mathbf{k}_V^- \left(\dot{\mathbf{w}}^{t+\Delta t} - \widehat{\mathbf{w}}^{t+\Delta t} \right) + \mathbf{B}^T \mathbb{F} \beta^{t+\Delta t} = 0 \quad (37)$$

where $\beta^{t+\Delta t}$ is the Lagrange multiplier.

The problem to solve at the linear stage becomes:

Find $(\mathbf{w}^{t+\Delta t}, \dot{\mathbf{w}}^{t+\Delta t}, \mathbf{f}^{t+\Delta t}, \beta^{t+\Delta t})$ solution to :

$$\begin{cases} \mathbf{K} \mathbf{u}^{t+\Delta t} = \mathbf{f}_d + \mathbf{N}^T \mathbf{f}^{t+\Delta t} \\ \mathbf{w}^{t+\Delta t} = \mathbf{N} \mathbf{u}^{t+\Delta t} \\ \mathbb{F}^T \mathbf{B} \dot{\mathbf{w}}^{t+\Delta t} = 0 \\ \mathbf{f}^{t+\Delta t} - \widehat{\mathbf{f}}^{t+\Delta t} + \mathbf{k}_V^- \left(\frac{\mathbf{w}^{t+\Delta t} - \mathbf{w}^t}{\Delta t} - \widehat{\mathbf{w}}^{t+\Delta t} \right) + \mathbf{B}^T \mathbb{F} \beta^{t+\Delta t} = 0 \end{cases} \quad (38)$$

4.3.3 Practical computation

Again, using the constraint in the search direction enables to find the expression of the Lagrange multiplier:

$$\beta^{t+\Delta t} = - \left(\mathbb{F}^T \mathbf{B} \mathbf{k}_V^- \mathbf{B}^T \mathbb{F} \right)^{-1} \mathbb{F}^T \mathbf{B} \left[\mathbf{k}_V^- \left(\mathbf{f}^{t+\Delta t} - \widehat{\mathbf{f}}^{t+\Delta t} \right) - \widehat{\mathbf{w}}^{t+\Delta t} \right] \quad (39)$$

The search direction thus reads:

$$\left(\mathbb{I} - \mathbf{Q}_M \right) \left(\mathbf{f}^{t+\Delta t} - \widehat{\mathbf{f}}^{t+\Delta t} \right) + \mathbf{k}_V^- \frac{\mathbf{w}^{t+\Delta t} - \mathbf{w}^t}{\Delta t} - \left(\mathbb{I} - \mathbf{Q}_M \right) \mathbf{k}_V^- \widehat{\mathbf{w}}^{t+\Delta t} = 0 \quad (40)$$

with $\mathbf{Q}_M = \mathbf{B}^T \mathbb{F} \left(\mathbb{F}^T \mathbf{B} \mathbf{k}_V^- \mathbf{B}^T \mathbb{F} \right)^{-1} \mathbb{F}^T \mathbf{B} \mathbf{k}_V^-$

Remark 7

- \mathbf{Q}_M is a macro projector. Like \mathbf{P}_M , it only depends on the initial search direction.
- The search direction enables to define the micro part of the force $(\mathbb{I} - \mathbf{Q}_M) \mathbf{f}^{t+\Delta t}$ as a function of the displacement.
- Note that the macro part of the force $\mathbf{Q}_M \mathbf{f}^{t+\Delta t}$ can be written as: $\mathbf{B}^T \mathbb{F} \gamma^{t+\Delta t}$

Thanks to the last remark, we split the force term in the equilibrium of the subdomains:

$$\mathbf{K} \mathbf{u}^{t+\Delta t} = \mathbf{f}_d + \mathbf{N}^T \underbrace{(\mathbb{I} - \mathbf{Q}_M) \mathbf{f}^{t+\Delta t}}_{\text{micro part via search direction}} + \mathbf{N}^T \underbrace{\mathbf{Q}_M \mathbf{f}^{t+\Delta t}}_{\text{macro part: } \mathbf{B}^T \mathbb{F} \gamma^{t+\Delta t}} \quad (41)$$

We have now a problem with two unknowns: $\gamma^{t+\Delta t}$ and $\mathbf{u}^{t+\Delta t}$. Using the search direction, we can express $\mathbf{u}^{t+\Delta t}$ as a function of $\gamma^{t+\Delta t}$. Then the weak global continuity enables to compute $\gamma^{t+\Delta t}$:

$$\begin{aligned} \gamma^{t+\Delta t} = & - \left(\mathbb{F}^T \mathbf{B} \mathbf{N} \left(\mathbf{K} + \mathbf{N}^T \frac{\mathbf{k}_V^-}{\Delta t} \mathbf{N} \right)^{-1} \mathbf{N}^T \mathbf{B}^T \mathbb{F} \right)^{-1} \mathbb{F}^T \mathbf{B} \mathbf{N} \left(\mathbf{K} + \mathbf{N}^T \frac{\mathbf{k}_V^-}{\Delta t} \mathbf{N} \right)^{-1} \dots \quad (42) \\ & \dots \left[\mathbf{f}_d + \mathbf{N}^T (\mathbb{I} - \mathbf{Q}_M) \left(\widehat{\mathbf{f}}^{t+\Delta t} + \mathbf{k}_V^- \widehat{\mathbf{w}}^{t+\Delta t} \right) + \mathbf{N}^T \frac{\mathbf{k}_V^-}{\Delta t} \mathbf{w}^t \right] \end{aligned}$$

And by re-injecting the expression of $\gamma^{t+\Delta t}$ in the equilibrium relation we obtain:

$$\left(\mathbf{K} + \mathbf{N}^T \frac{\mathbf{k}_V^-}{\Delta t} \mathbf{N} \right) \mathbf{u}^{t+\Delta t} = (\mathbb{I} - \mathbf{R}) \left[\mathbf{f}_d + \mathbf{N}^T (\mathbb{I} - \mathbf{Q}_M) \left[\widehat{\mathbf{f}}^{t+\Delta t} + \mathbf{k}_V^- \widehat{\mathbf{w}}^{t+\Delta t} \right] + \mathbf{N}^T \frac{\mathbf{k}_V^-}{\Delta t} \mathbf{w}^t \right] \quad (43)$$

with $\mathbf{R} = \mathbf{N}^T \mathbf{B}^T \mathbb{F} \left(\mathbb{F}^T \mathbf{B} \mathbf{N} \left(\mathbf{K} + \mathbf{N}^T \frac{\mathbf{k}_V^-}{\Delta t} \mathbf{N} \right)^{-1} \mathbf{N}^T \mathbf{B}^T \mathbb{F} \right)^{-1} \mathbb{F}^T \mathbf{B} \mathbf{N} \left(\mathbf{K} + \mathbf{N}^T \frac{\mathbf{k}_V^-}{\Delta t} \mathbf{N} \right)^{-1}$

Remark 8

- For the case of perfect interface $\mathbf{B} \widehat{\mathbf{w}}^{t+\Delta t} = \mathbf{B} \widehat{\mathbf{w}}^t = 0$ so $\mathbf{Q}_M \widehat{\mathbf{w}}^{t+\Delta t} = 0$ and the problem to be solved becomes:

$$\left(\mathbf{K} + \mathbf{N}^T \frac{\mathbf{k}_V^-}{\Delta t} \mathbf{N} \right) \mathbf{u}^{t+\Delta t} = (\mathbb{I} - \mathbf{R}) \left[\mathbf{f}_d + \mathbf{N}^T (\mathbb{I} - \mathbf{Q}_M) \widehat{\mathbf{f}}^{t+\Delta t} + \mathbf{N}^T \left[\mathbf{k}_V^- \widehat{\mathbf{w}}^{t+\Delta t} + \mathbf{N}^T \frac{\mathbf{k}_V^-}{\Delta t} \mathbf{w}^t \right] \right] \quad (44)$$

- We see that the weak global continuity does not affect the Robin condition. It only modifies the right-hand side. Anyhow it allows to propagate the information related to the load on the whole structure.

5 Numerical examples

A first comparison between a mono-scale and a multiscale implementation is presented in 5.1 on a 3D traction beam case. The impact of the multiscale approach for both approaches is illustrated. A 3D industrial contact case is finally presented to illustrate the compatibility of the multiscale approach with contact interfaces.

5.1 Comparison between a mono and a multiscale implementation

The comparison between the mono-scale and the multiscale strategy is performed on the case of a 3D homogeneous isotropic linear elastic beam decomposed in 8, 16, 32, 64 and 128 subdomains. The Young modulus is E , Poisson ratio ν , the length of the beam L and section S . The parameters are given in Table 1. Figure 7 presents a comparison between a mono-scale and the multiscale implementation with the global equilibrium strategy.

On Figure 7a, the dependency of the convergence with respect to the substructuring is shown. The more subdomains the structure is split into, the more iterations are required to reach the same level of convergence. After 70 iterations the ratio of the error indicator between a 8 and 128 substructuring is 100. On Figure 7b we illustrate the impact of the multiscale strategy. The convergence is much less dependent on the substructuring and it is much faster than in the mono-scale implementation. For

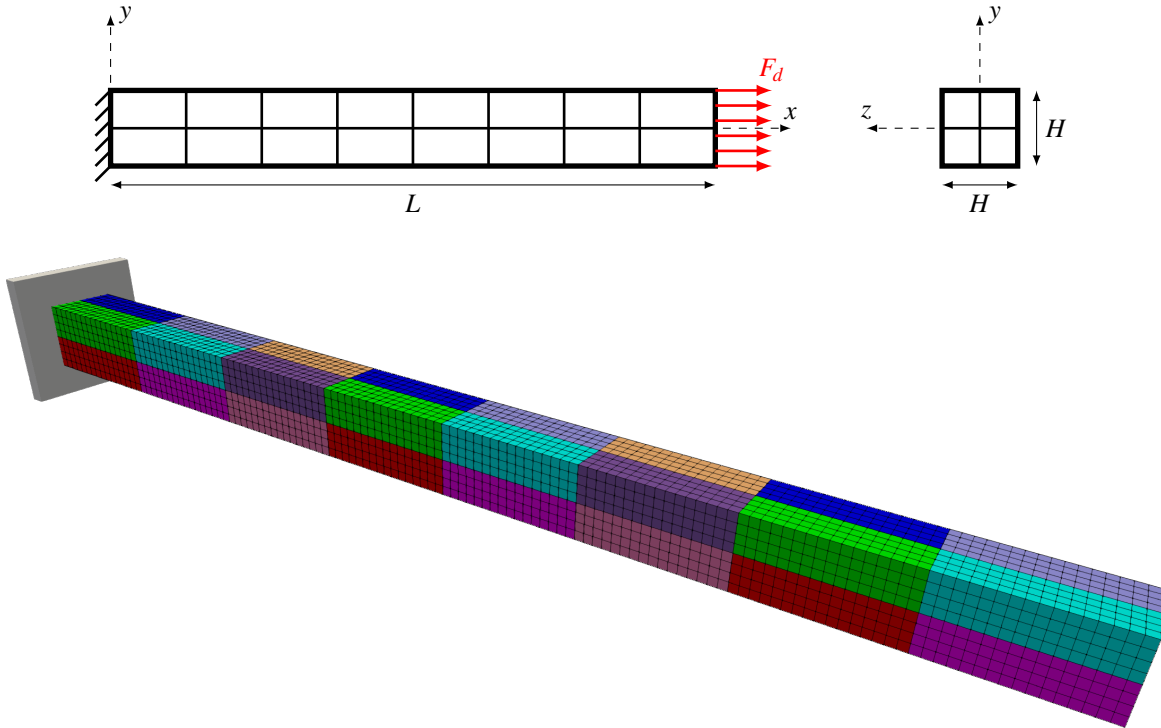


Figure 6: substructured traction beam

Table 1: Parameters

Parameters	Value/Range
Young Modulus Y	200 GPa
Young Modulus of soles Y_S	$0.008Y$
ν	0.3
Length L	160 mm
Section S	10×10 mm
Load F_d	10 MPa
Size mesh h	1.25 mm
substructuring	8,16,32,64,128

example the indicator of 10^{-5} is reached after 50 iterations for the 8-substructure beam in mono-scale whereas only 7 iterations are required for the 32-substructure beam with the multiscale method.

Even if the convergence is still better than for the mono-scale approach, the strategy with global continuity is not scalable as can be seen on figure 7c. Indeed the global continuity manages to spread the right-hand side on all the subdomains, but it does not couple the local equilibriums together as the weak balance does (the Robin condition is not modified by the constraint).

Figures 8a and 8b show the deformation and tension states after one iteration for the two multiscale approaches on a 332-subdomain decomposition. In that example where the solution is a uniform tension, we observe that the global balance leads to a quasi exact solution (in stress) after initialization; the global continuity leads to a better looking solution but the correct stress state is far from being found. After the second iteration, on Figures 9a and 9b, the global balance is almost converged (the stress state at the interface is a visualization artifact) whereas the global continuity is far from the solution.

Remark 9 *With the global balance approach, after few iterations all that remains to be found is orthogonal to the macro constraint and thus a classical (slow) fixed point convergence rate is achieved.*

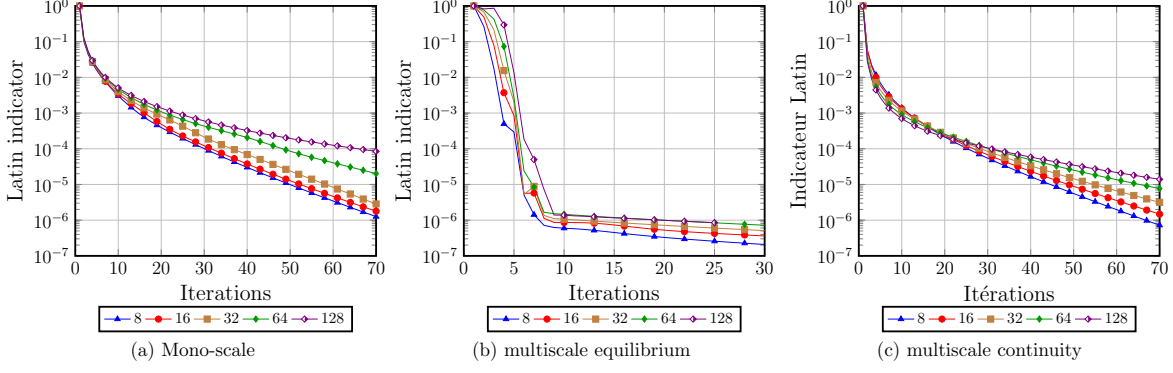


Figure 7: Comparison for different weighting of the search direction - Latin indicator

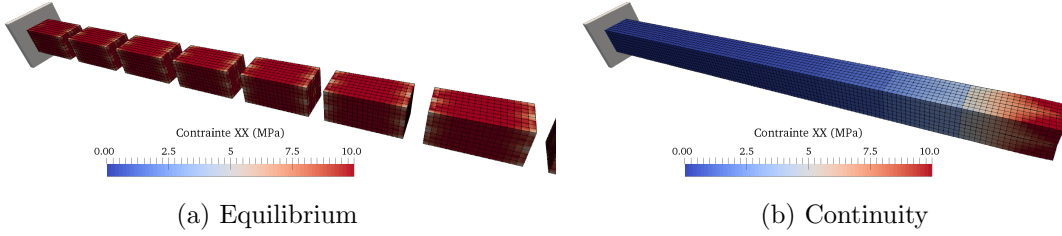


Figure 8: Iteration 1 for the multiscale approaches

5.2 Impact of the search direction on the multiscale approach

We now study the impact of the search direction on the convergence of the multiscale approach for a beam substructured in 32 subdomains. To do so, the reference Young modulus of the soles will be multiplied by 0.01, 0.1, 10 and 100. We present the different convergence curves in term of jump of displacement and equilibrium of forces (Figure 10). Such results can be easily interpreted by considering the two following limit cases about the search direction:

- the case when $\mathbf{k} \rightarrow \infty$: with such an assumption the search direction can be considered equivalent to:

$$\dot{\mathbf{w}}^{t+\Delta t} - \widehat{\mathbf{w}}^{t+\Delta t} + \mathbf{A}^T \mathbb{W} \alpha^{t+\Delta t} = 0 \quad (45)$$

Such a search direction improves the convergence of the displacements. Indeed as forces have disappeared, the displacement of linear stage become closer than the displacement from local stage which is naturally continuous. Conversely, the convergence of the interface forces is deteriorated. However through the multiscale approach it still remains acceptable.

- The case when $\mathbf{k} \rightarrow 0$: with such an assumption the search direction can be considered equivalent to :

$$\mathbf{f}^{t+\Delta t} - \widehat{\mathbf{f}}^{t+\Delta t} = 0 \quad (46)$$

In addition of the multiscale effect, such a search direction implies that the forces are quasi-equilibrated. However the search direction no more includes displacements and their convergence is deteriorated.

From these considerations and from Figure 10, the initial choice of the search direction seems to manage a good compromise.

Results of the continuity strategy are shown on Figure 11. A similar analysis for the asymptotic search direction than the equilibrium strategy can be done. When the weighting decreases, the convergence of the force term is improved whereas the jump of displacement stagnates very quickly. On the other hand, increasing the weighting disturbs the convergence of the force since displacement terms

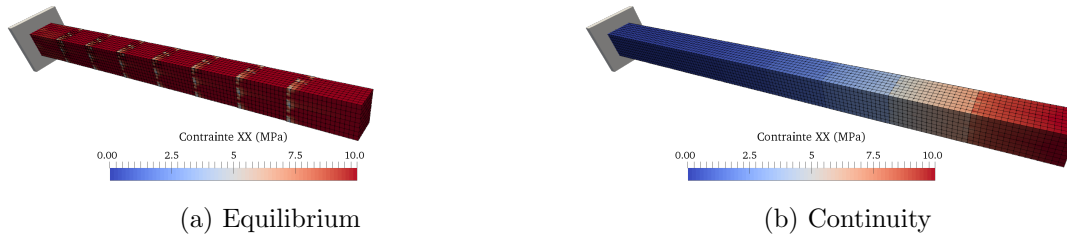


Figure 9: Iteration 2 for the multiscale approaches

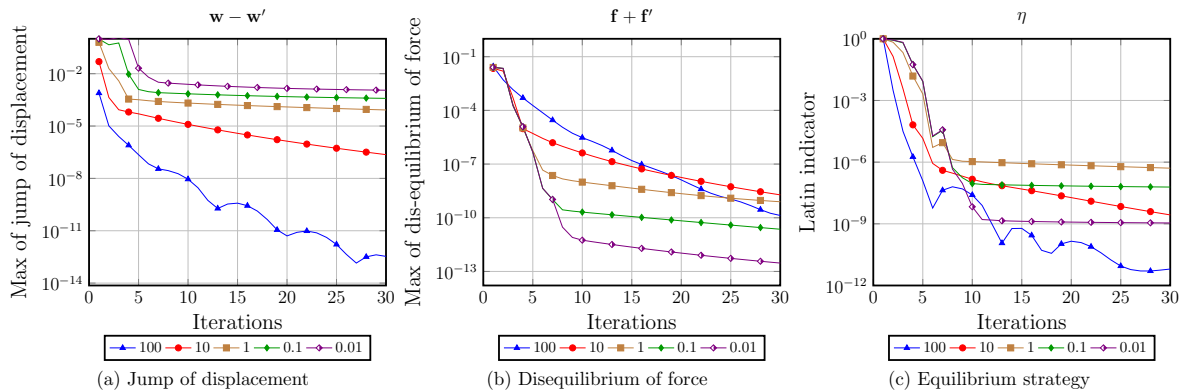


Figure 10: Comparison for different weighting of the search direction - Equilibrium strategy

dominate in the search direction. However too much weighting does not seem to increase particularly the convergence of the displacement.

5.3 A study of the speed-up

We present in this section the results about the speed-up of the method. We use again the 3D beam structure presented previously. The beam consists of 25 millions degrees of freedom. The error criterion to stop the computation is chosen at 10^{-5} . Each subdomain is computed on one CPU. On the figure 12, we present the speed-up in term of CPU time for the several substructuring. The speed-up is computed in comparison with the CPU time with 16 subdomains. The gain due to parallel processing is very poor for the mono-scale approach. Due to the non-scalability, the more subdomains there are, the more iterations are required to reach the same level of error. In the case of the multiscale approach with global equilibrium, the scalability almost permits to reach the theoretical speed-up. However, with too many subdomains, the speed-up will grow slower because of the many communications to do between substructures. This phenomenon is already visible for 128 subdomains.

5.4 A 3D multi-contact problem with friction

In this part, the objective is to prove the robustness of the Latin method in presence of many contact interfaces. In order to illustrate this robustness, we choose a polycrystalline structure where all the interfaces between the grains are considered to be contact interfaces with friction. Each grain is made of iron with $E = 200\text{GPa}$ and $\nu = 0.3$. In total, the structure is blend of 100 substructures linked by 467 interfaces. The structure is a cube which consists of 565 000 degrees of freedom (Figure 13a), blocked on the bottom face and loaded on the top face. The load is applied in 4 steps (Figure 13b). The Coulomb coefficient is 0.1 for all the interfaces. We use the multiscale approach with a global equilibrium.

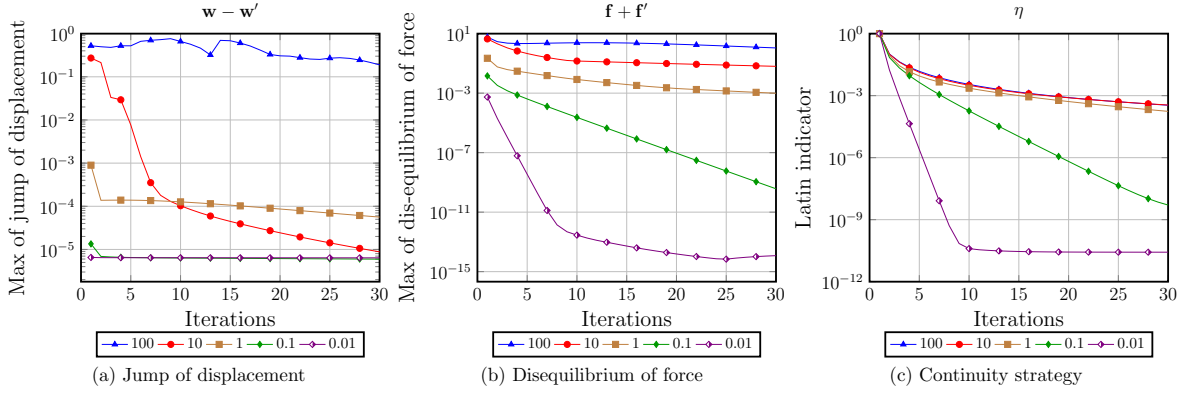


Figure 11: Comparison for different weighting of the search direction - Continuity strategy

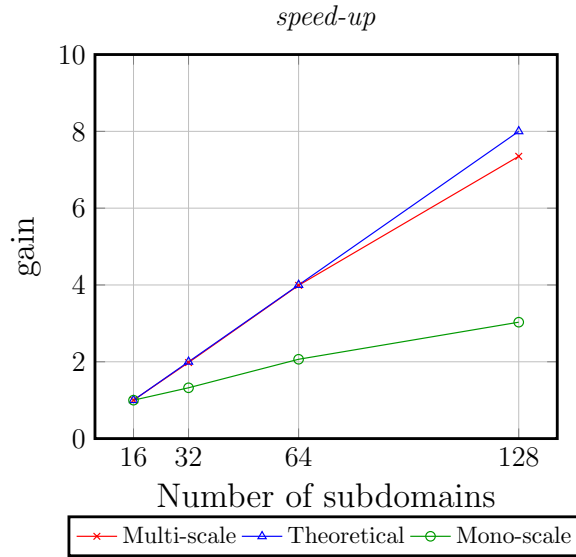


Figure 12: Comparison of the speed-up

5.4.1 Convergence

The figure 14 shows the deformed shapes of the structure at the different load-steps. During the first two load-steps, more and more sliding appears between the subdomains. Due to the weak Coulomb coefficient, detachment between subdomains is observed during the unload (two last load-steps). Of course, at the end of the load sequence, the structure does not go recover to its initial shape because of the sliding and detachment.

The figure 15 shows a comparison of the evolution of the error indicator during the iterations between the mono-scale strategy and the multiscale approach for a global equilibrium. On the first iterations, the impact of the multiscale approach is obvious. After few iterations (around 5) the multiscale approach does not bring any more information and the convergence rate is similar to the monoscale approach.

5.4.2 Details of time computation

We present here some details about the time spent to simulate this structure with the multiscale approach. We compare some functions by considering the smallest and the largest subdomains, described in table 2.

The table 3 presents the details of the principal functions. As the smallest subdomain has 3 times less interfaces than the largest and almost 8 times less nodes on the interfaces, its local stage is faster ($\times 5.6$). Even though its linear stage begins earlier, it has to wait for all other subdomains to exchange

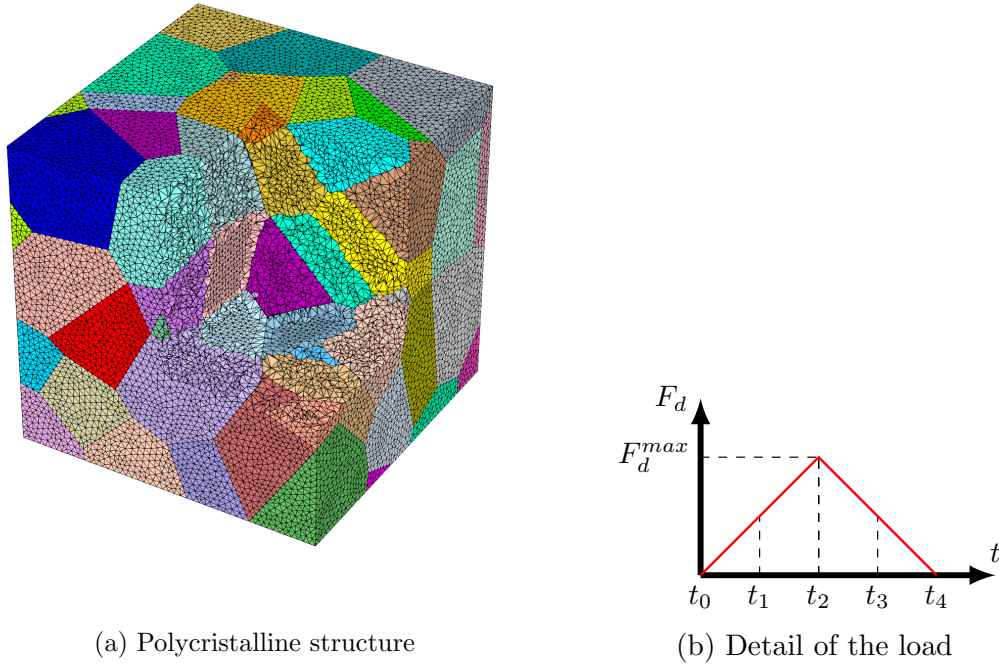


Figure 13: Polycrystalline structure and load

Table 2: Comparison between the smallest and biggest subdomains

	Smallest subdomain	Largest subdomain
Nodes of the subdomain	529	5639
Nodes on the interfaces	160	1258
Number of interfaces	5	18

the results of the first step of the macro strategy. The MPI communications are described on table 4. The smallest subdomain spends almost 80% of its time to wait for other subdomains. This explains the longer duration of the linear stage for the smallest subdomain. A communication hiding procedure [3] will be considered in the future.

As a global reduction is also needed for the computation of the convergence indicator, the time of computation of the associated function is equivalent whatever the subdomain. However, due to the specific management of the memory of the industrial code `code_aster`, this function occupies a non-negligible part of the global time computation. This time is directly linked to the size of the subdomain and the number of associated interfaces.

The little remaining percents in the table 3 principally correspond to minor functions for post-processing and `mpi.sendrecv` communications to neighbors between the linear stage and the local stage.

	Smallest subdomain			Largest subdomain		
	#calls	Time (s)	ratio	#calls	Time (s)	ratio
Local stage	70	1766	4.84%	70	9964	27.3%
Linear stage	70	26341	72.2%	70	15954	43.7%
Indicator computation	70	5200	14.2%	70	4677	12.8%
Memory management	70	828	2.3%	70	4944	13.5%
Total			92.5%			97.3%

Table 3: Time repartition for the principal functions

This simulation illustrates issues due to the lack of balance of size between the subdomains. The

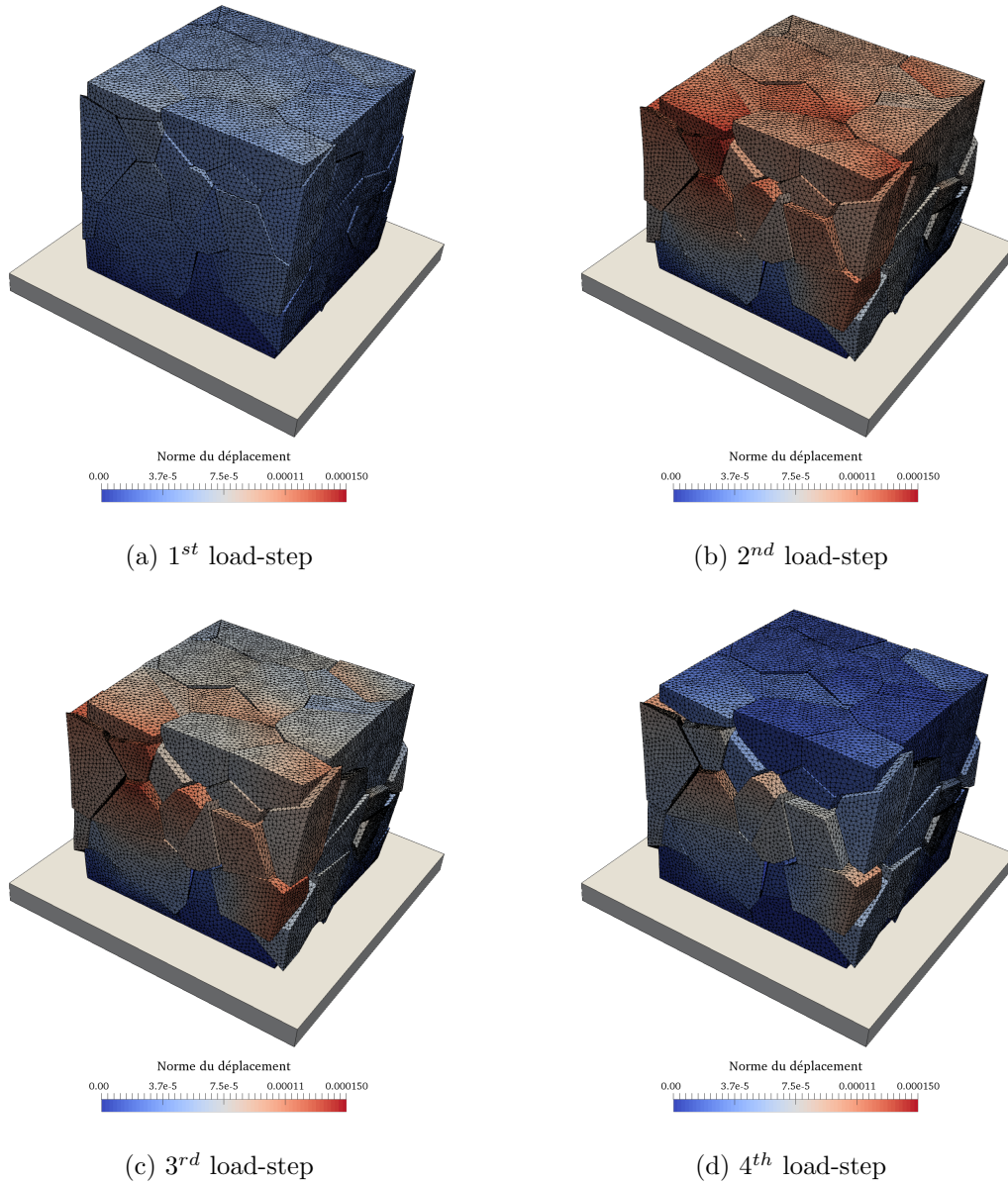


Figure 14: Deformed shape according the load-steps

	Smallest subdomain			Largest subdomain		
	#calls	Time (s)	Global Part	#calls	Time (s)	Global part
Python mpi.allreduce	630	28615	78.4%	630	815	2.2%
Python mpi.sendrecv	1750	1385	3.8%	6300	37	0.1%

Table 4: Time repartition for MPI communications

small subdomains have to wait for the large ones. A simple solution is to re-split large subdomains into pieces connected by perfect interfaces. In the future, we will also consider asynchronous iterations [24, 23, 22] to allow small subdomains to continue their iterations even in the absence of information from large subdomains.

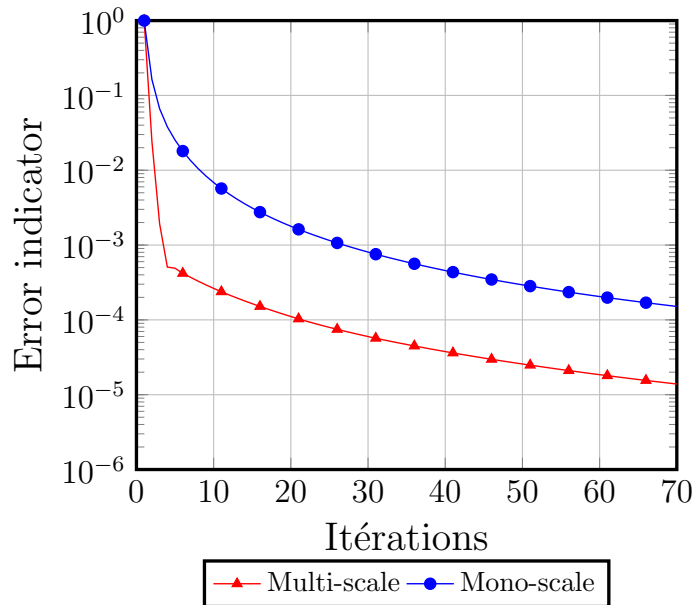


Figure 15: Error indicator

6 Conclusion and perspectives

In this paper a non-invasive implementation of a multiscale mixed domain decomposition has been presented. The introduction of a multiplier to enforce a global equilibrium of force distribution is seen as a low-rank softening of the mono-scale search direction which weakly couples neighboring subdomains together.

A “dual” macro approach has been proposed to enforce a global continuity of displacements instead of a global equilibrium of force. The computational strategy stays similar to the global equilibrium approach: the two-level algorithm consists in a first parallel computation over subdomains before a global correction that transmits the macro information. However this approach appears not to be scalable. Contrary to the equilibrium approach, it is not possible to interpret it as a modification of the mono-scale search direction.

A 3D structure involving many interfaces with frictional contact and 565 000 degrees of freedom has been studied. The multiscale and the monoscale approaches have been compared with obvious advantage for the multiscale strategy. For this computation, the subdomains matched the parts in contact (no subdivision of large subdomains was considered), leading to strong lack of load balancing and idling small subdomains.

As observed in the examples, the multiscale approach only accelerates the convergence during the first iterations, we are currently working on acceleration strategies in order to avoid the plateau that is observed later.

References

- [1] O. Bettinotti, O. Allix, U. Perego, V. Oancea, and B. Malherbe. A fast weakly intrusive multi-scale method in explicit dynamics. *International Journal for Numerical Methods in Engineering*, 100:577–595, 2014.
- [2] M. Blanchard, O. Allix, P. Gosselet, and G. Desmeure. Mastering the convergence of the global-local non-invasive coupling technique in viscoplasticity. *Finite Element Analysis and Design*, x:submitted, 2017.
- [3] S. Cools and W. Vanroose. The communication-hiding pipelined bicgstab method for the parallel solution of large unsymmetric linear systems. *Parallel Computing*, 65(Supplement C):1 – 20, 2017.

- [4] M. Duval, J. C. Passieux, M. Salaün, and S. Guinard. Non-intrusive Coupling: Recent Advances and Scalable Nonlinear Domain Decomposition. *Archives of Computational Methods in Engineering*, 23(1):17–38, 2016.
- [5] C. Farhat, P.-S. Chen, and J. Mandel. A scalable lagrange multiplier based domain decomposition method for time-dependent problems. *International Journal for Numerical Methods in Engineering*, 38(22):3831–3853, 1995.
- [6] C. Farhat and J. Mandel. The two-level FETI method for static and dynamic plate problems Part I: An optimal iterative solver for biharmonic systems. *Computer Methods in Applied Mechanics and Engineering*, 155(1-2):129–151, mar 1998.
- [7] C. Farhat, J. Mandel, and F. Roux. Optimal convergence properties of the FETI domain decomposition method. *Computer Methods in Applied Mechanics and Engineering*, 115(3-4):365–385, 1994.
- [8] C. Farhat and F.-X. Roux. A method of finite element tearing and interconnecting and its parallel solution algorithm. *International Journal for Numerical Methods in Engineering*, 32(6):1205–1227, 1991.
- [9] M. J. Gander. Optimized Schwarz Methods. *SIAM Review*, 44(2):699–731, 2006.
- [10] L. Gendre, O. Allix, and P. Gosselet. Non-intrusive and exact global/local techniques for structural problems with local plasticity. *Computational Mechanics*, 44:233–245, 2009.
- [11] P. Gosselet, D. Rixen, F.-X. Roux, and N. Spillane. Simultaneous-FETI and Block-FETI: robust domain decomposition with multiple search directions. *International Journal for Numerical Methods in Engineering*, 104(10):905–927, 2015.
- [12] P.-A. Guidault, O. Allix, L. Champaney, and C. Cornuault. A multiscale extended finite element method for crack propagation. *Computer Methods in Applied Mechanics and Engineering*, 197(5):381–399, 2008.
- [13] A. Klawonn, P. Radtke, and O. Rheinbach. FETI-DP Methods with an Adaptive Coarse Space. *SIAM Journal on Numerical Analysis*, 53(1):297–320, 2015.
- [14] L. Y. Kolotilina. Twofold deflation preconditioning of linear algebraic systems. i. theory. *Journal of Mathematical Sciences*, 89(6):1652–1689, 1998.
- [15] Y. A. Kuznetsov. Algebraic multigrid domain decomposition methods. *Russian Journal of Numerical Analysis and Mathematical Modelling*, 4(5):351–380, 1989.
- [16] Y. A. Kuznetsov. Multigrid domain decomposition methods for elliptic problems. *Computer methods in applied mechanics and engineering*, 75(1-3):185–193, 1989.
- [17] P. Ladevèze. *Nonlinear computational structural mechanics: new approaches and non-incremental methods of calculation*. Mechanical Engineering Series. Springer-Verlag, New-York, 1999.
- [18] P. Ladevèze and D. Dureisseix. Une nouvelle stratégie de calcul micro/macro en mécanique des structures. *Comptes Rendus de l'Académie des Sciences - Series IIB - Mechanics-Physics-Astronomy*, 327(12):1237–1244, nov 1999.
- [19] P. Ladevèze, O. Loiseau, and D. Dureisseix. A micro–macro and parallel computational strategy for highly heterogeneous structures. *International Journal for Numerical Methods in Engineering*, 52(12):121–138, sep 2001.
- [20] P. Ladevèze and A. Nouy. On a multiscale computational strategy with time and space homogenization for structural mechanics. *Computer Methods in Applied Mechanics and Engineering*, 192(28-30):3061–3087, jul 2003.
- [21] O. Loiseau. *Une stratégie de calcul multiéchelle pour les structures hétérogènes*. PhD thesis, Ecole Normale Supérieure de Cachan, 2001.

- [22] F. Magoulès and G. Gbikpi-Benissan. JACK: an asynchronous communication kernel library for iterative algorithms. *Journal of Supercomputing*, pages 1–20, 2016.
- [23] F. Magoulès and C. Venet. Asynchronous iterative sub-structuring methods. *Mathematics and Computers in Simulation*, 2016.
- [24] F. Magoulès, D. B. Szyld, and C. Venet. Asynchronous optimized schwarz methods with and without overlap. Technical report, Research Report 15-06-19, Department of Mathematics, Temple University, 2015.
- [25] J. Mandel and M. Brezina. Balancing domain decomposition: Theory and performance in two and three dimensions. Technical report, University of Colorado at Denver, Denver, CO, USA, 1993.
- [26] J. Mandel and B. Sousedík. Adaptive selection of face coarse degrees of freedom in the bddc and the feti-dp iterative substructuring methods. *Computer methods in applied mechanics and engineering*, 196(8):1389–1399, 2007.
- [27] J. Mandel, B. Sousedík, and J. Šístek. Adaptive BDDC in three dimensions. *Mathematics and Computers in Simulation*, 82(10):1812–1831, jun 2012.
- [28] F. Nataf, H. Xiang, V. Dolean, and N. Spillane. A Coarse Space Construction Based on Local Dirichlet-to-Neumann Maps. *SIAM Journal on Scientific Computing*, 33(4):1623–1642, 2011.
- [29] R. A. Nicolaides. Deflation of conjugate gradients with applications to boundary value problems. *SIAM Journal on Numerical Analysis*, 24(2):355–365, 1987.
- [30] P. Oumaziz, P. Gosselet, P.-A. Boucard, and S. Guinard. A non-invasive implementation of a mixed domain decomposition method for frictional contact problems. *Computational Mechanics*, 60(5):797–812, Nov 2017.
- [31] J. C. Passieux, J. Réthoré, A. Gravouil, and M. C. Baietto. Local/global non-intrusive crack propagation simulation using a multigrid X-FEM solver. *Computational Mechanics*, 52(6):1381–1393, 2013.
- [32] C. Pechstein and C. R. Dohrmann. A unified framework for adaptive bddc. Technical report, Technical Report 2016-20, Johann Radon Institute for Computational and Applied Mathematics (RICAM), 2016.
- [33] Y. Saad, M. Yeung, J. Erhel, and F. Guyomarc’h. A deflated version of the conjugate gradient algorithm. *SIAM Journal on Scientific Computing*, 21(5):1909–1926, 2000.
- [34] K. Saavedra, O. Allix, P. Gosselet, J. Hinojosa, and A. Viard. An enhanced nonlinear multi-scale strategy for the simulation of buckling and delamination on 3D composite plates. *Computer Methods in Applied Mechanics and Engineering*, 317:952–969, 2017.
- [35] N. Spillane and D. J. Rixen. Automatic spectral coarse spaces for robust FETI and BDD algorithms. *Internat. J. Num. Meth. Engin.*, 95(11):953–990, 2013.
- [36] J. M. Tang, R. Nabben, C. Vuik, and Y. A. Erlangga. Comparison of Two-Level Preconditioners Derived from Deflation, Domain Decomposition and Multigrid Methods. *Journal of Scientific Computing*, 39(3):340–370, 2009.
- [37] P. Wesseling. Introduction to multigrid methods. Technical report, DTIC Document, 1995.
- [38] M. A. Woodbury. Inverting modified matrices. *Memorandum report*, 42(106):336, 1950.